Size and Semiconducting Effects on the Piezoelectric Performances of ZnO Nanowires Grown onto Gravure-Printed Seed Layers on Flexible Substrates

Andrés Jenaro Lopez Garcia [1], Thomas Jalabert [1], Manojit Pusty [1], Viktor Defoor [1], Xavier Mescot [1], Maria Montanino [2], Giuliano Sico [2], Fausta Loffredo [2], Fulvia Villani [2], Giuseppe Nenna [2] and Gustavo Ardila [1,*]

[1] Université Grenoble Alpes, CNRS, Grenoble INP, IMEP-LaHC, F-38000 Grenoble, France; andres-jenaro.lopez-garcia@grenoble-inp.fr (A.J.L.G.); thomas.jalabert@grenoble-inp.fr (T.J.); manojit.pusty@grenoble-inp.fr (M.P.); viktor.defoor@hotmail.com (V.D.); xavier.mescot@imep.grenoble-inp.fr (X.M.)

[2] ENEA Portici Research Center, p.le Enrico Fermi 1, 80055 Portici, NA, Italy; maria.montanino@enea.it (M.M.); giuliano.sico@enea.it (G.S.); fausta.loffredo@enea.it (F.L.); fulvia.villani@enea.it (F.V.); giuseppe.nenna@enea.it (G.N.)

* Correspondence: ardilarg@minatec.grenoble-inp.fr

PFM DataCube mode uses the force volume method to perform simultaneously electrical and mechanical measurements. In this mode, the data is continuously recorded while the tip is in contact with the sample. However, the tip is retracted each time it is moved laterally to avoid lateral bending of the NWs. For a single pixel, data acquisition is divided into three steps: i) First, the tip is approached to get in contact with the surface (see Figure S1a). During this step (around 50 ms), there is no deflection of the cantilever or piezoresponse signal (see Figure S1b-d). ii) Once the cantilever reaches a given deflection setpoint (20 nm in this example), [1]the tip height is frozen (for a dwell time of 80 ms), and the piezoresponse amplitude and phase are recorded (with a sampling rate of 204 values). During the last step iii), the tip is withdrawn from the surface, reducing both the cantilever deflection and the piezoresponse signals as shown in Figure S1b-d before moving to the next pixel. The piezoresponse amplitude and phase were averaged from 20 frames taken randomly from the step ii) using Nanoscope Analysis software and Python programming language. A single image in both amplitude and phase were compiled as shown in Figure S1e and f.

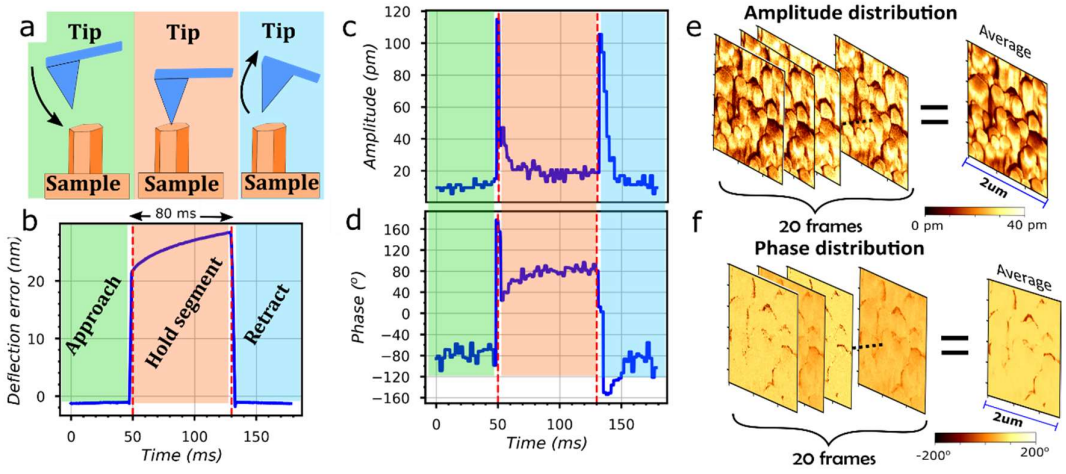

Figure S1. PFM DataCube mode. (**a**) Schematics of PFM DataCube procedure during which at each pixel position, the tip is approached from the sample surface, held at a fixed height, and then retracted. (**b**) Deflection curve of the cantilever. (**c**) Piezoresponse amplitude and (**d**)

piezoresponse phase during data acquisition in one pixel. (**e**) Averaged amplitude and (**f**) averaged phase maps after data treatment of 20 frames.

PFM measurements were performed at three different positions of each sample (with different substrates and annealing times) (see Figure S2a). These measurements allowed us to verify the reproducibility of their piezoelectric behavior. Figure S2c shows the piezoresponse amplitude histograms for each position, together with a fit constituted of the sum of four Gaussian fits. As discussed in the main text, these four contributions to the piezoresponse amplitude are related to different NW radius and border effects. Figure S2c displays the black, blue, green, and purple Gaussian mean values for each spot. The piezoresponse amplitudes are the same in every place, indicating the presence of homogeneous piezoelectric properties throughout the sample. Consequently, all the data of piezoelectric amplitude histograms from the different spots are collected in a single histogram reflecting the piezoelectric properties of the sample (see the bottom histogram in Figure S2c).

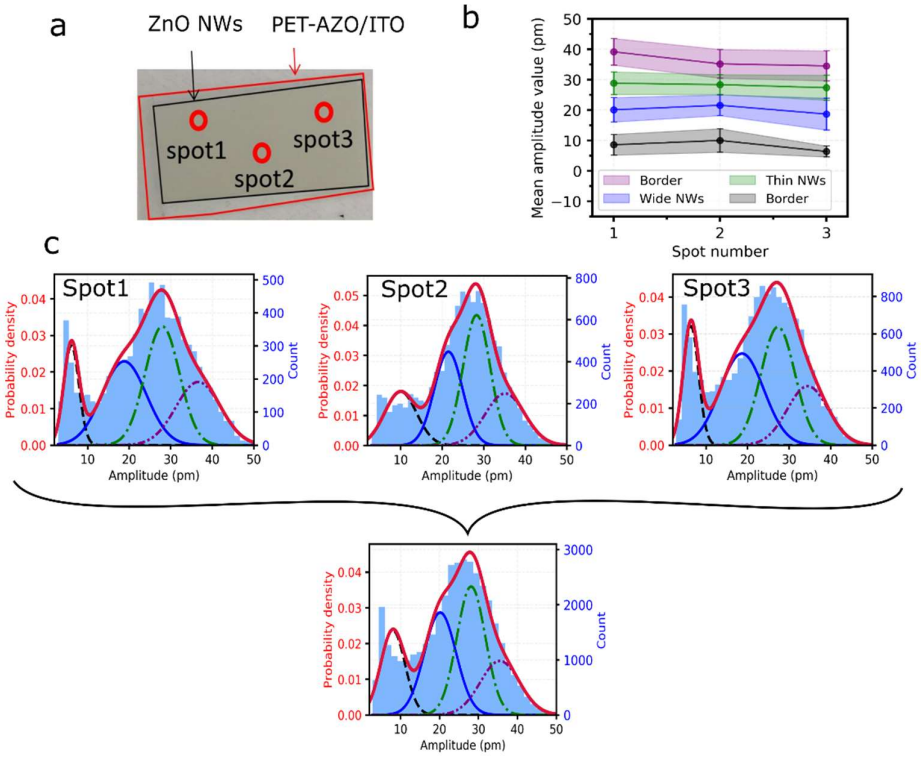

Figure S2. Piezoresponse amplitude histograms at different locations on the same sample. (**a**) Position of the three random spots where PFM measurements were performed. (**b**) Mean piezoelectric amplitude extracted from Gaussian fit for the three different positions shown in (**a**). (**c**) Piezoresponse amplitude histogram of these three spots and final amplitude data adding the contributions of all spots. The sample is constituted of ZnO NWs grown on PET-AZO with an annealing time of 2.5 h. Measurements are performed with a 5 V piezoelectric drive at 13 kHz.

The piezoelectric and semiconducting properties of ZnO required to perform the simulations presented in the main text are taken from literature and collected in Table S1.

Table S1. Piezoelectric and semiconductor properties of ZnO used for the numerical simulation.

ZnO properties	Symbol	Value	References
Elastic constants	C_{11}	209.7 GPa	[44]
	C_{12}	121.1 GPa	
	C_{13}	105.1 GPa	
	C_{33}	210.9 GPa	
	C_{44}	42.47 GPa	
	C_{66}	42.29 GPa	
Piezoelectric coefficients	e_{13}	$-0.51\ \mathrm{C/m^2}$	[45]
	e_{33}	$-1.22\ \mathrm{C/m^2}$	
	e_{15}	$-0.45\ \mathrm{C/m^2}$	
Dielectric constants	κ_{11}	7.77	[46]
	κ_{33}	8.91	
Doping level	N_d	$5 \cdot 10^{17}\mathrm{cm^{-3}}$	[30]
Band gap energy level	E_g	3.37 eV	[47]

Figure S3 and Figure S4 show topography and PFM measurements carried on all samples with different annealing times and substrates. This data allowed us to perform the analysis discussed in main text. The measurements for 1 h annealing time are shown on the main text. The piezoresponse amplitude and phase distributions are extracted from these measurement and are displayed in Figure S5 and Figure S6. The amplitude histograms are fitted with Gaussian curves in the same fashion as in the main text (i.e., four Gaussians corresponding to the contributions of different NW sizes). The mean values of each Gaussian curve are plotted in Figure S7.

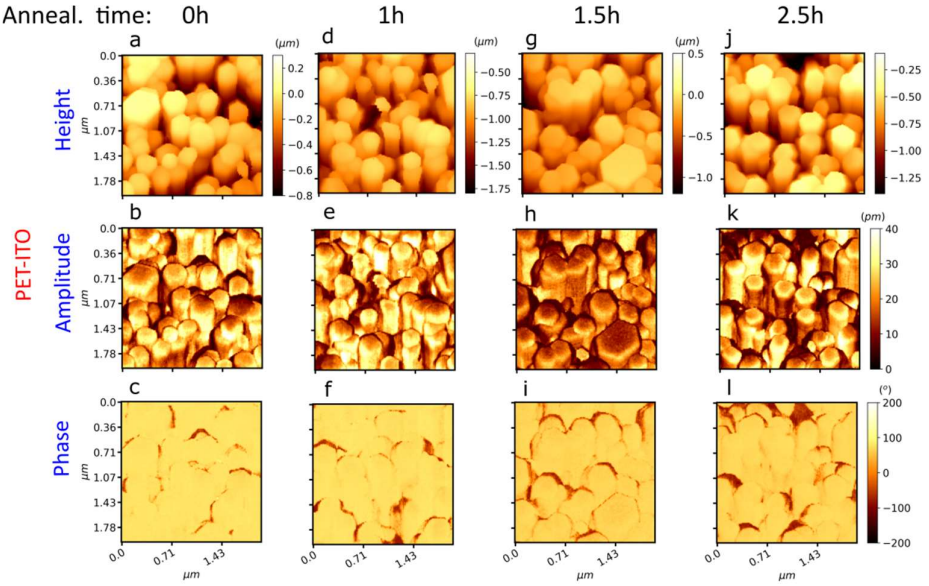

Figure S3. Topography, amplitude and phase distributions on ZnO NWs grown on PET-ITO substrate for annealing times of (**a**-**c**) 0 h, (**d**-**f**) 1 h, (**g**-**i**) 1.5 h and (**j**-**l**) 2.5 h.

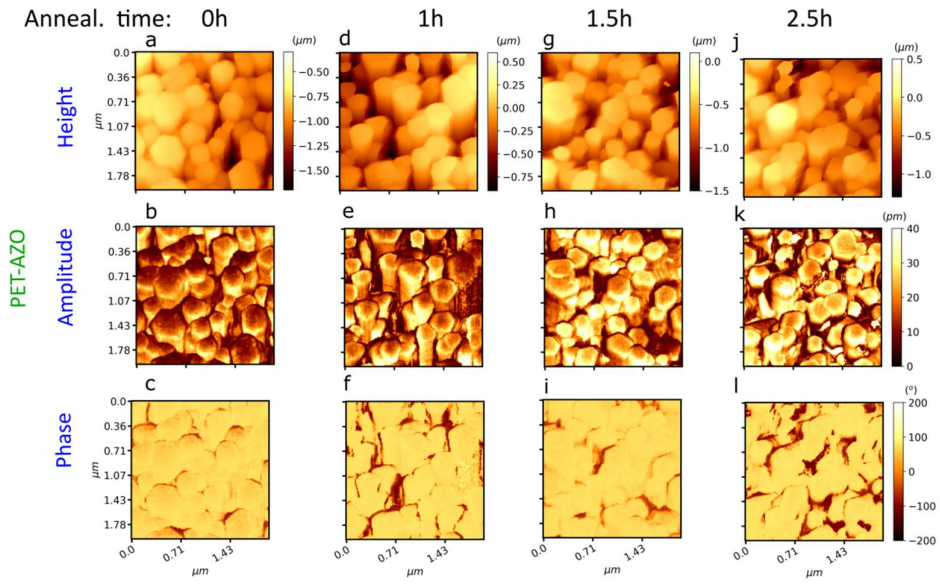

Figure S4. Topography, amplitude, and phase distributions on ZnO NWs grown on PET-AZO substrate for annealing times of (a-c) 0 h, (d-f) 1 h, (g-i) 1.5 h, and (j-l) 2.5 h.

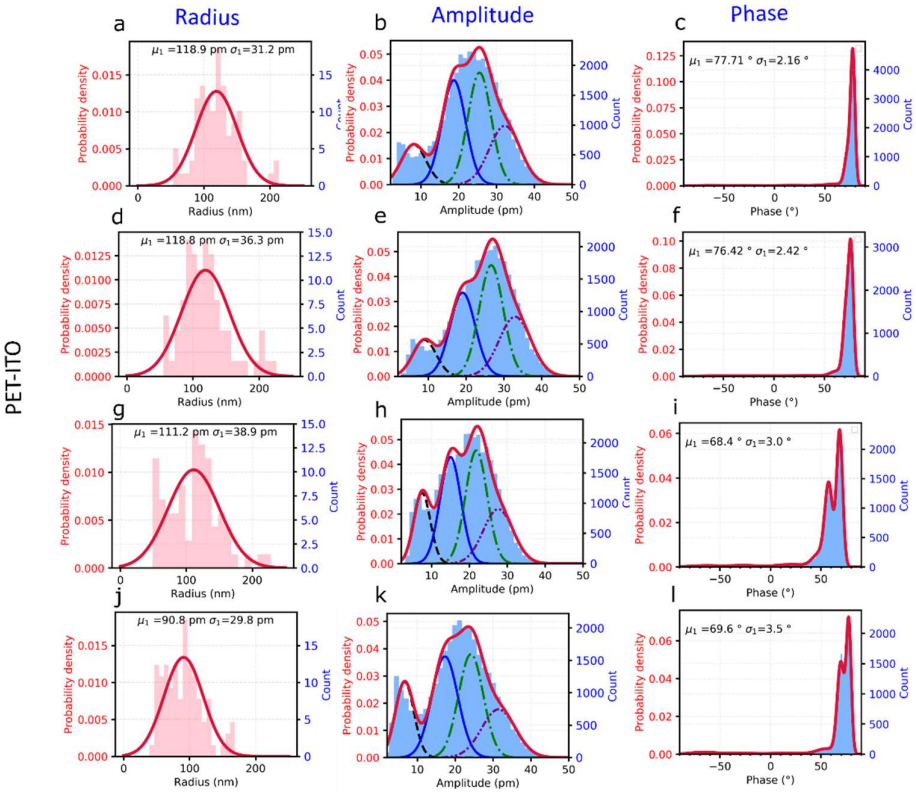

Figure S5. Histograms of ZnO NW radius, piezoelectric amplitude, and piezoelectric phase values for samples over PET-ITO substrates with an annealing time of (**a-c**) 0 h, (**d-f**) 1 h, (**g-i**) 1.5 h and (**j-l**) 2.5 h. In amplitude graphs, from left to right, black, blue, green, and purple Gaussian fits correspond to different NW sizes and border effects (see Figure S2).

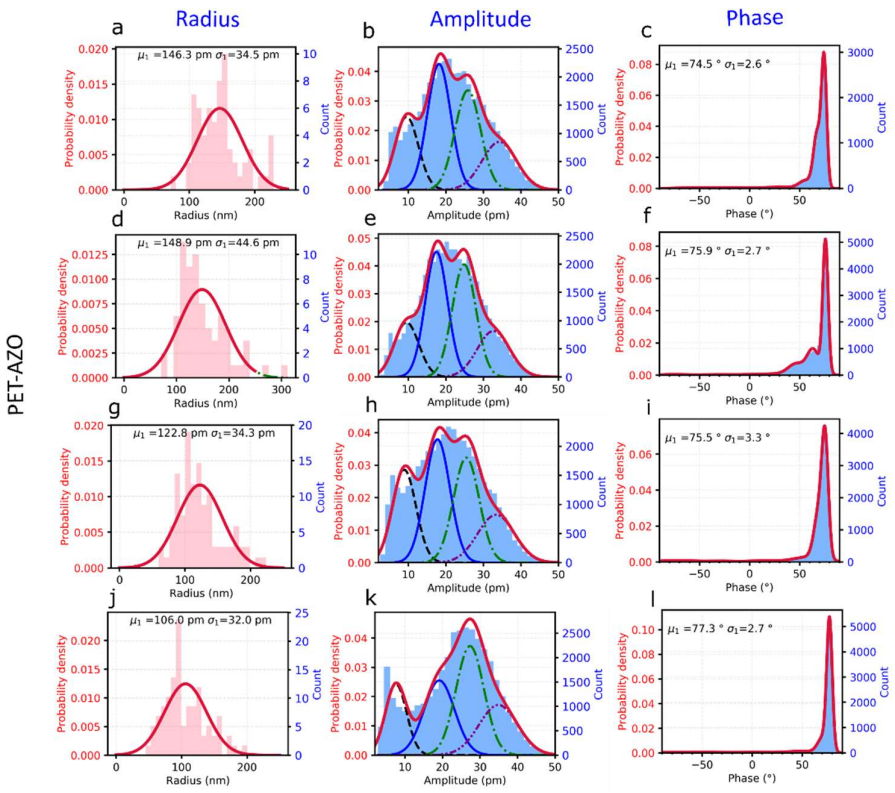

Figure S6. Histograms of ZnO NWs radius, piezoelectric amplitude, and piezoelectric phase values for samples over PET-AZO substrates with an annealing time of (**a**-**c**) 0 h, (**d**-**f**) 1 h, (**g**-**i**) 1.5 h and (**j**-**l**) 2.5 h. In amplitude graphs, from left to right, black, blue, green, and purple Gaussian fits correspond to different NW sizes and border effects (see Figure S2).

Using all AFM topography maps from each PFM measurement, we extracted the NWs radius distributions for each annealing time and substrate (see Figure S5 and S6). The average NW radius slightly decreases with the annealing time, from 146 nm to 107 nm for PET-AZO and from 118 to 90 nm for PET-ITO. It is worth noticing that the average NW radius is always smaller on PET-ITO than on PET-AZO substrates.

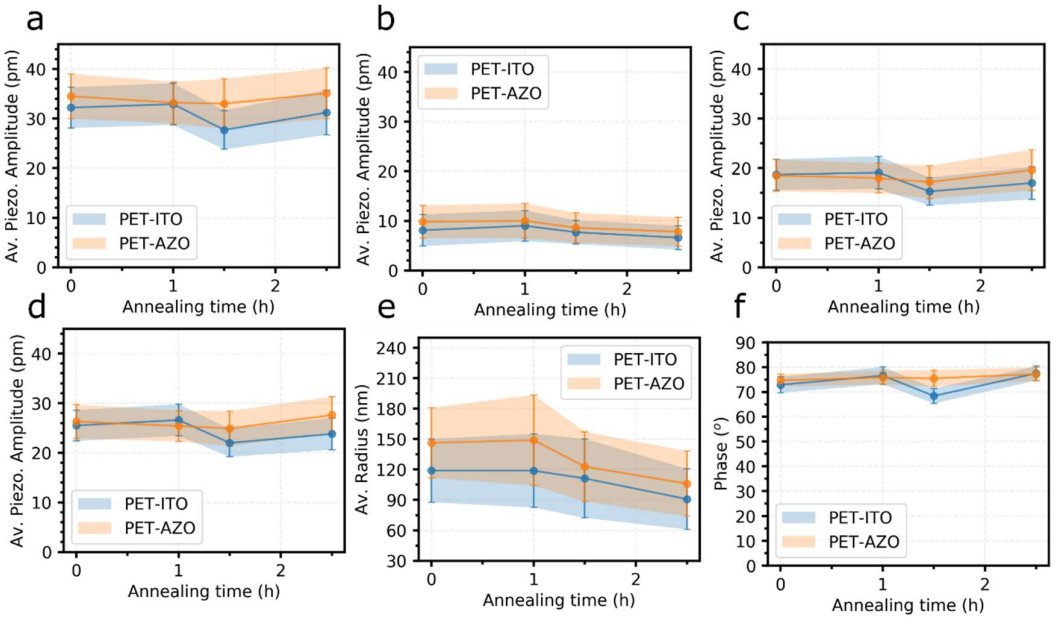

Figure S7. The mean value of the piezoelectric amplitude as a function of annealing time, in both PET-ITO and PET-AZO substrates, from (a), (b) the border effect contributions, (c) the thin, and (d) the wide ZnO NWs contributions. (e) ZnO radius as a function of the annealing time in both ITO and AZO seed layer and (f) the mean value of the piezoelectric phase.

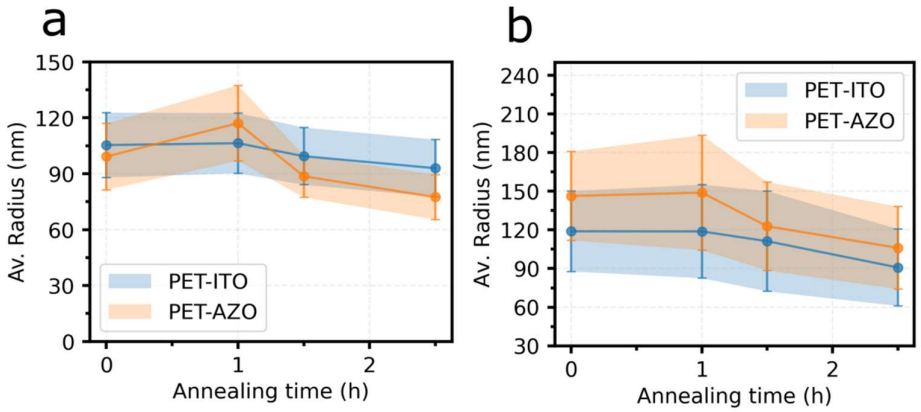

Figure S8. Mean value of radius extracted from (**a**) SEM measurements (**b**) AFM measurements.

The NW radii extracted from AFM measurements are about 40 nm larger than those extracted from SEM measurements (see Figure S7). We think that this is due to convolution effects between the AFM tip and the NWs. Following [48], we compute the convolution error considering the probe radius of 25 nm (r_{tip}) and the measured width (w_{exp}) for the wide NW of 200 nm radius. For a value of height contact equal to r_{tip} (25 nm), the convolution error approximately $2*r_{tip}$ = 50 nm, in agreement with the difference observed between SEM and AFM measurements.

References

44. Bateman, T.B. Elastic Moduli of Single-Crystal Zinc Oxide. *J. Appl. Phys.* **1962**, *33*, 3309–3312. https://doi.org/10.1063/1.1931160.

45. Carlotti, G.; Socino, G.; Petri, A.; Verona, E. Acoustic Investigation of the Elastic Properties of ZnO Films. *Appl. Phys. Lett.* **1987**, *51*, 1889–1891. https://doi.org/10.1063/1.98502.
46. Ashkenov, N.; Mbenkum, B.N.; Bundesmann, C.; Riede, V.; Lorenz, M.; Spemann, D.; Kaidashev, E.M.; Kasic, A.; Schubert, M.; Grundmann, M.; et al. Infrared Dielectric Functions and Phonon Modes of High-Quality ZnO Films. *J. Appl. Phys.* **2003**, *93*, 126–133. https://doi.org/10.1063/1.1526935.
30. Lopez Garcia, A.J.; Mouis, M.; Consonni, V.; Ardila, G. Dimensional Roadmap for Maximizing the Piezoelectrical Response of ZnO Nanowire-Based Transducers: Impact of Growth Method. *Nanomaterials* **2021**, *11*, 941. https://doi.org/10.3390/nano11040941.
47. Look, D.C.; Reynolds, D.C.; Sizelove, J.R.; Jones, R.L.; Litton, C.W.; Cantwell, G.; Harsch, W.C. Electrical Properties of Bulk ZnO. *Solid State Commun.* **1998**, *105*, 399–401. https://doi.org/10.1016/S0038-1098(97)10145-4.
48. Canet-Ferrer, J.; Coronado, E.; Forment-Aliaga, A.; Pinilla-Cienfuegos, E. Correction of the Tip Convolution Effects in the Imaging of Nanostructures Studied through Scanning Force Microscopy. *Nanotechnology* **2014**, *25*, 395703; doi:10.1088/0957-4484/25/39/395703.